SUPPLEMENT TO THE *WELDING JOURNAL*, JANUARY 2013
Sponsored by the American Welding Society and the Welding Research Council

Interfacial Microstructure of Diode Laser Brazed AZ31B Magnesium to Steel Sheet Using a Nickel Interlayer

The formation of a nano-scale Fe(Ni) transition layer on the steel during laser brazing was found to be responsible for the formation of a metallurgical bond between the steel and magnesium

BY A. M. NASIRI, D. C. WECKMAN, AND Y. ZHOU

ABSTRACT

The brazeability of AZ31B-H24 magnesium alloy and steel sheet with a microlayer of electro-deposited Ni in a single flare bevel lap joint configuration has been investigated. The macro- and microstructure, element distribution, and interfacial phases of the joints were studied by optical microscopy (OM), scanning electron microscopy (SEM), transmission electron microscopy (TEM), and X-ray diffraction (XRD). Wetting of the steel by the Mg-Al brazing alloy was improved significantly through the addition of a Ni electroplated interlayer. Bonding between the magnesium brazing alloy and the steel was facilitated by the formation of a transition layer composed of a solid solution of Ni in Fe on the steel followed by a layer of α-Mg + Mg_2Ni eutectic. A band of AlNi intermetallic compound with different morphologies also formed along the steel-fusion zone interface, but was not directly responsible for bonding. Ni electroplating was found to significantly improve the brazeability and mechanical performance of the joint. The average fracture shear strength of the bond reached 96.8 MPa and the joint efficiency was 60% with respect to the AZ31B-H24 Mg alloy base metal. In all cases, failure occurred in the fusion zone very close to the steel-fusion zone interface.

Introduction

Prized for its excellent strength-to-weight ratio, magnesium and its alloys are currently under intense investigation for use in many applications in the automotive and aerospace industries (Refs. 1–3). However, steel sheet is still the most commonly used material in the automotive industry for fabrication of autobody structures. The ability to make hybrid structures of magnesium alloy and steel sheet would be desirable for many applications in the automotive industry, because the overall weight of the autobody could be reduced resulting in better fuel efficiencies and lower environmental impact. Therefore, there is increasing interest in identifying and developing new techniques and processes that can be used to make dissimilar joints between magnesium alloys and steel sheet (Refs. 3–9).

Joining magnesium alloys to steel by conventional fusion welding technologies is difficult due to the large difference in the melting points between Mg (649°C) and Fe (1538°C). In addition, the boiling point of magnesium is only 1091°C, so direct contact with molten steel causes catastrophic vaporization of the magnesium (Refs. 3–8). Moreover, the maximum solid solubility of Fe in Mg is estimated to be only 0.00041 at.-% Fe (Ref. 6) and wetting of steel by molten magnesium is very poor (Ref. 8).

The weldability of magnesium to steel using the hybrid laser-arc welding (Refs. 5, 6, 8, 9) and resistance spot welding (Refs. 4, 7) processes has been examined. Zhao et al. (Ref. 5) used a hybrid laser-gas tungsten arc welding (GTAW) process to join AZ31B magnesium alloy and 304 stainless steel. However, oxides that formed at the interface were found to cause joints with poor tensile strength. Using the same welding technique, Liu et al. (Refs. 8, 9) studied lap joining of AZ31B Mg alloy to Q235 steel with Sn and Cu interlayers. Mg_2Sn and Mg_2Cu intermetallic compounds were found to form along the grain boundaries of the Mg alloy when using the Sn and Cu interlayers, respectively. The use of Sn and Cu interlayers was reported as the main reason for the elimination of gaps along the steel-fusion zone interface and the improvement of wetting properties of the steel by molten magnesium alloy (Refs. 8, 9). Finally, in a recent study, Liu et al. (Refs. 4, 7) used resistance spot welding to join AZ31B magnesium alloy to DP600 Zn-coated steel. They found that a preexisting transition layer of Fe_2Al_5 between the Zn coating and the steel improved wetting and bonding between the steel and the magnesium alloy.

Review of the literature suggests that joining Mg alloys to steel will be possible provided the temperatures required for joining are kept below the boiling point of the magnesium alloy (1091°C) and provided another interlayer element is used that can interact and promote wetting and bonding between both immiscible alloys. For this reason, brazing can be a superior choice in joining dissimilar metals such as magnesium and steel because brazing

*A. M. NASIRI (*amnasiri@uwaterloo.ca*), D. C. WECKMAN, and Y. ZHOU are with Department of Mechanical & Mechatronics Engineering, Centre for Advanced Materials Joining, University of Waterloo, Waterloo, ON, Canada.*

KEYWORDS

Laser Brazing
AZ31B Mg Sheet
Steel Sheet
Dissimilar
Intermetallic Compound

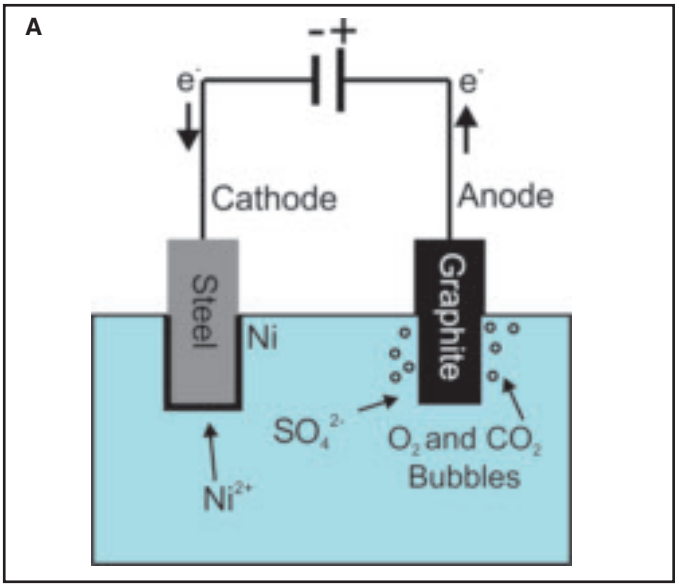

Fig. 1— A — Schematic of the Ni electrodeposition process on steel; B — transverse section of the Ni electrodeposited layer on the steel substrate.

temperatures are generally lower than the melting points of both base metals. In addition, very fast heating and cooling rates can be used during the brazing process to minimize the thickness of intermetallic compounds that might form along the interfaces (Ref. 10).

The benefits of using laser brazing and laser welding-brazing technologies for joining dissimilar materials are also becoming increasingly recognized due to the combined attributes of furnace brazing and laser welding (Ref. 11). With a more localized energy input and more precise control of the laser beam energy, high joining speeds and accompanying high cooling rates can be realized with minimal heating of the parts. Also, laser brazing and laser welding-brazing can prevent or minimize excessive formation of detrimental intermetallic phases. If intermetallic layers can be limited to thicknesses below 10 µm, acceptable joint strengths and mechanical properties may be obtained (Refs. 12–14).

In our previous study (Ref. 15), a diode laser brazing process was developed for joining Mg alloy sheet to aluminized steel sheet where the Al-12Si coating served as the interlayer. This coating was found to promote wetting of the steel by the magnesium brazing alloy; however, a preexisting layer of brittle θ-$FeAl_3$ along the braze-steel interface was found to degrade the mechanical properties of the joint as failure of the joint always occurred by fracture of this brittle intermetallic layer. Following a review of binary and ternary phase diagrams, nickel was identified as a potentially viable interlayer element between the steel and Mg-9Al-2Zn brazing alloy used. Therefore, the purpose of this present study was to investigate the brazeability, interfacial microstructure, and mechanical properties of the laser brazed AZ31B-H24 magnesium alloy to steel sheet with an electrodeposited layer of Ni on the steel to act as the interlayer element. It is expected that development of this laser brazing technology for joining of steel-interlayer-Mg alloy combinations with a strong metallurgical bond between the steel and Mg alloy will facilitate increased application and use of Mg alloys in the automotive industry.

Experimental Procedure

In this study, 2-mm-thick commercial-grade twin-roll strip cast AZ31B-H24 Mg alloy sheet and 1-mm-thick steel sheet were used as the base materials. The chemical compositions of the base materials are given in Tables 1 and 2. A 2.4-mm-diameter TiBraze Mg 600 filler metal (Mg-Al-Zn alloy) with solidus and liquidus temperatures of 445° and 600°C, respectively, was chosen for this study. The commercial flux used in the experiments was Superior No. 21 manufactured by Superior Flux and Manufacturing Co. This powder flux was composed of LiCl (35–40 wt-%), KCl (30–35 wt-%), NaF (10–25 wt-%), NaCl (8–13 wt-%), and $ZnCl_2$ (6–10 wt-%) (Ref. 16).

The AZ31B Mg and steel sheets were cut into 60- × 50-mm specimens. Prior to laser brazing, the oxide layers on the surfaces of the magnesium sheets were removed by stainless steel wire brushing. All the specimens were ultrasonically cleaned in acetone to remove oil and other contaminants from the specimen surfaces.

The edge of each steel sheet was bent in order to make a single-flare bevel lap joint after clamping against the magnesium sheet. After bending, the steel specimens were cleaned in acetone and then ground to 1000 grit using SiC abrasive paper and again ultrasonically cleaned in acetone. The prepared surfaces were then immediately electroplated with electrolytic pure nickel. In the Ni electroplating process, the clean steel sample was the cathode and graphite was the anode. The composition of the electroplating solution and the electroplating conditions are listed in Table 3. Figure 1A shows a schematic of the Ni electrodeposition process used. In order to get a uniform 5-µm-thick Ni layer on the steel, different cathode current densities and plating times were tested. Electrodeposition of Ni using a cathode current density of 120 mA/cm^2 for 10 min was found to provide a

Table 1 — Measured Chemical Composition of the AZ31-H24 Mg Alloy Sheet and TiBraze Mg 600 Filler Metal (wt-%)

	Al	Zn	Mn	Si	Mg
AZ31B-H24	3.02	0.80	0.30	0.01	Bal.
TiBraze Mg 600	9.05	1.80	0.18	—	Bal.

Table 2 — Measured Chemical Composition of the 1-mm-Thick Steel Sheet (wt-%)

C	0.01
Mn	0.5
P	0.010
S	0.005
Fe	Bal.

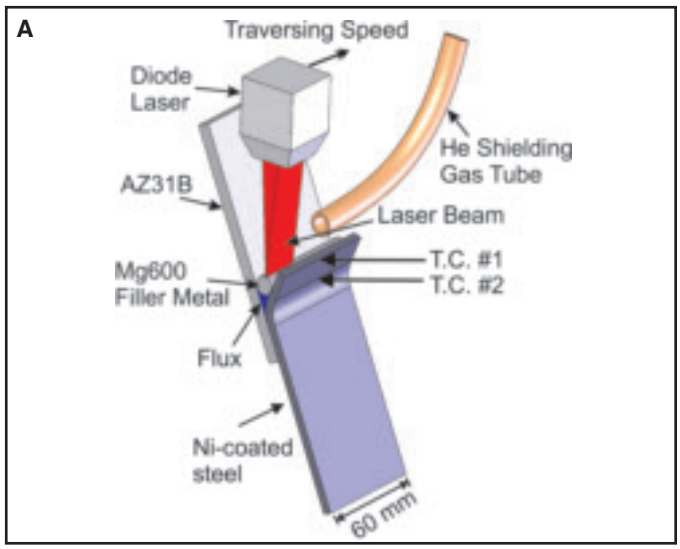

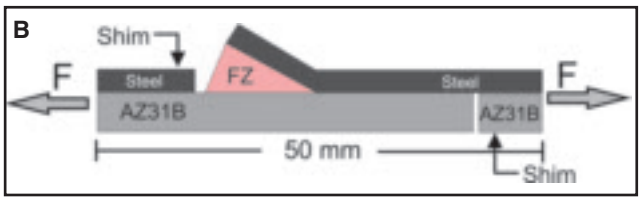

Fig. 2 — A — Schematic of the laser brazing system used for joining AZ31 Mg and Ni electro-plated steel sheets in the single-flare bevel lap joint configuration showing the position of two thermocouples used for temperature measurements; B — schematic of the 5-mm-wide tensile shear test specimen.

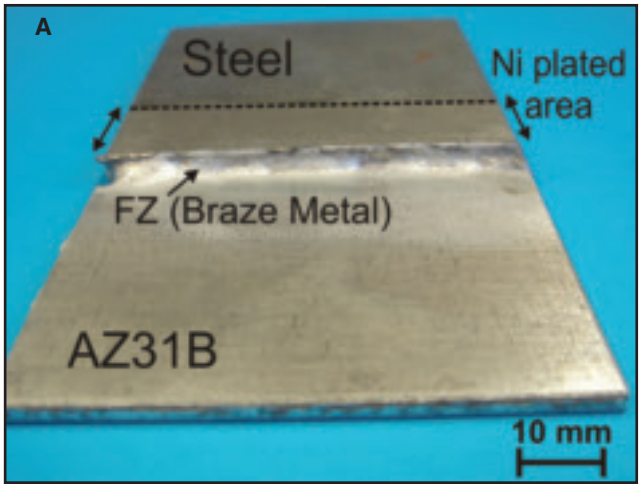

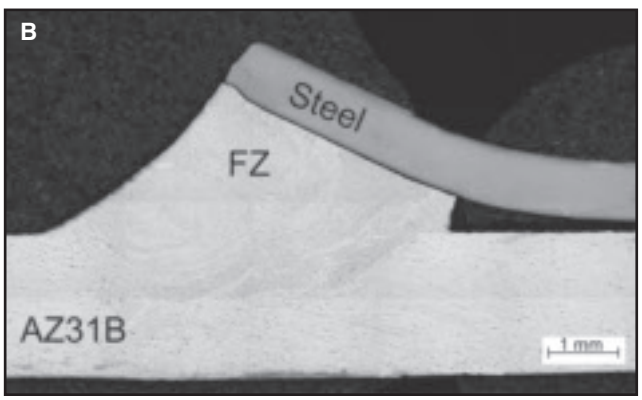

Fig. 3 — A laser-brazed Ni electroplated steel/AZ31B joint made using 8 mm/s travel speed and 2.2-kW laser beam power: A — Top bead; B — transverse section of the joint.

5.5 ± 0.9-μm-thick pure Ni coating layer on the steel with a defect-free interface. Figure 1B shows a SEM micrograph of the cross section of the nickel-coated steel. The white layer on top of the steel is the Ni coating layer. The coating was of uniform thickness with a void-free interface. Energy-dispersive X-ray spectrometer (EDS) analysis of the electrodeposited layer on the steel showed a pure Ni coating layer.

After the electroplating process, the prebent steel sheet was clamped against the magnesium sheet to make a single-flare bevel lap joint as shown in Fig. 2A. The filler metal was cut into pieces and preset on the workpiece at the weld interface with some flux before heating and brazing by the laser beam.

An integrated Panasonic 6-axis robot and Nuvonyx diode laser system with a maximum power of 4.0 kW and a 0.5- × 12-mm rectangular laser beam intensity profile at the focal point was used for laser brazing. This energy distribution is more suitable for brazing processes compared with the nonuniform Gaussian-distributed circular beams generated by CO_2 and Nd:YAG lasers (Ref. 17). The beam was focused on top of the filler metal.

In order to limit oxidation, helium shielding gas was provided in front of the molten pool with a flow rate of 30 L/min from a 6-mm-diameter soft copper feeding tube. Laser brazing was performed using a range of laser powers, travel speeds, and beam offset positions.

After laser brazing, transverse cross sections of the brazed specimens were cut and mounted in epoxy resin. The samples were then mechanically polished using 300, 600, 800, 1000, and 1200 grades of SiC grinding papers followed by polishing using a 1-μm diamond suspension. The polished specimens were etched to reveal the microstructure of the braze metal and AZ31B base material. The etchant was comprised of 20 mL acetic acid, 3 g picric acid, 50 mL ethanol, and 20 mL water (Ref. 18).

Macro- and microstructures of the etched joints were examined using an optical metallographic microscope. The microstructure and composition of different zones of the joint cross section were determined using a JEOL JSM-6460 scanning electron microscope (SEM) and EDS. Phase characterization of the phases formed in the steel-fusion zone interface and on the fracture surfaces was carried out using X-ray diffraction (XRD) phase analysis in a Rigaku AFC-8 diffractometer with Cu target, 50 kV acceleration voltage, and 40 mA current.

A transmission electron microscope (TEM) foil of the steel-fusion zone interfacial region was prepared using a focused ion beam (FIB) and in-situ lift out technique. After attaching the TEM foil to a copper grid, final thinning was performed on the sample at an acceleration voltage of 30 kV, followed by 10 kV, and 1 kV for the final polishing step to get a 100-nm-thick TEM sample. The TEM studies were performed with a JEOL 2010F TEM

Table 3 — Composition of Ni Electroplating Solution and Electroplating Parameters

Plating Solution Composition (g/L)	
$NiSO_4 \cdot 6H_2O$	263
Na_2SO_4	215
H_3BO_3	31

Electrodeposition Parameters	
Cathode current density	45–120 mA/cm^2
Time	5–20 min
pH	3
Temperature	25°C
Anode	Graphite (8 cm^2)
Cathode	Carbon Steel (6 cm^2)

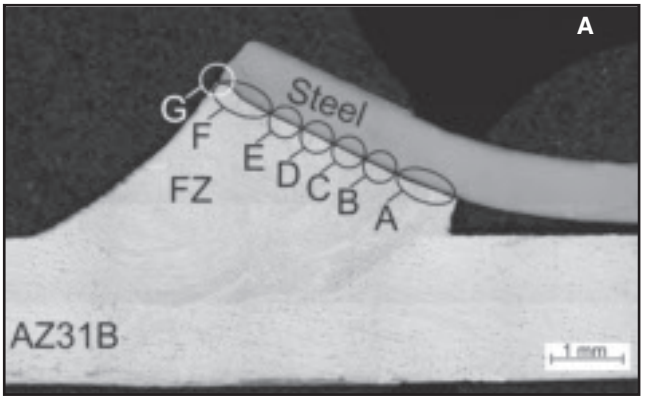

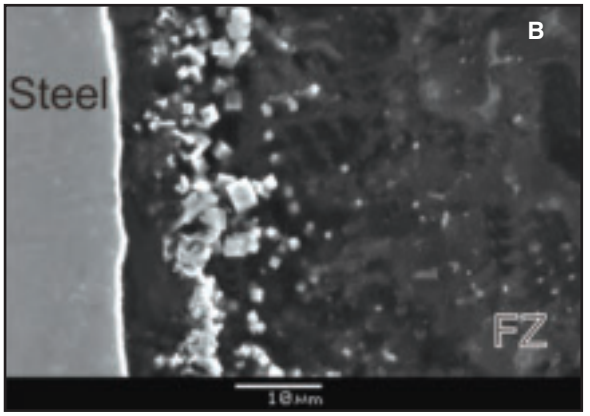

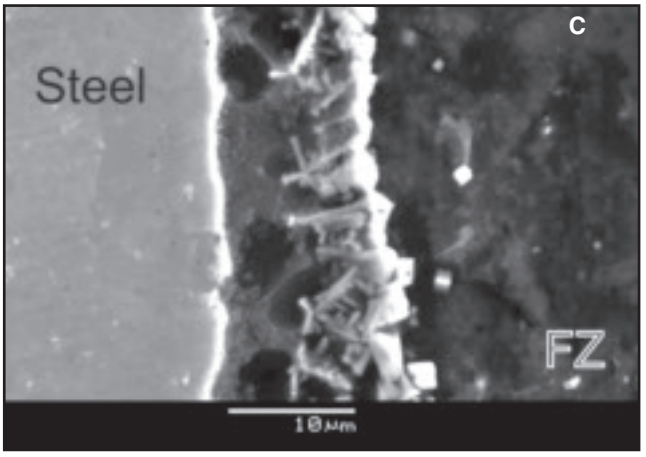

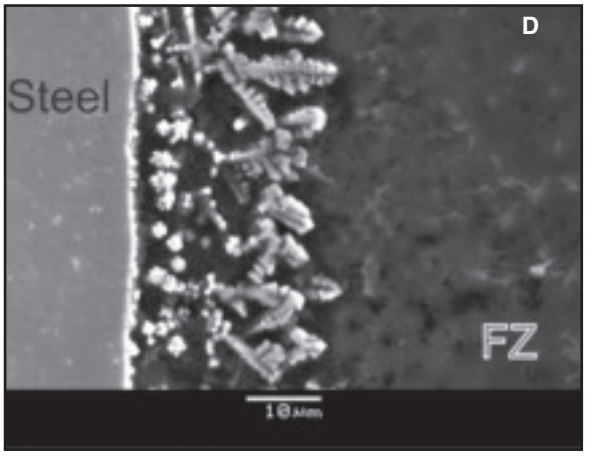

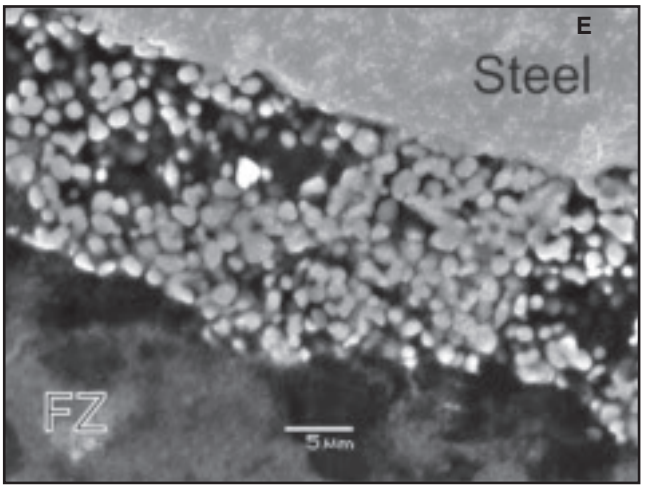

Fig. 4 — Transverse sections of a laser brazed joint. A — Optical micrograph of the entire joint and SEM images in different positions along the steel-FZ interface; B — position A; C — position C; D — position E; E — position F.

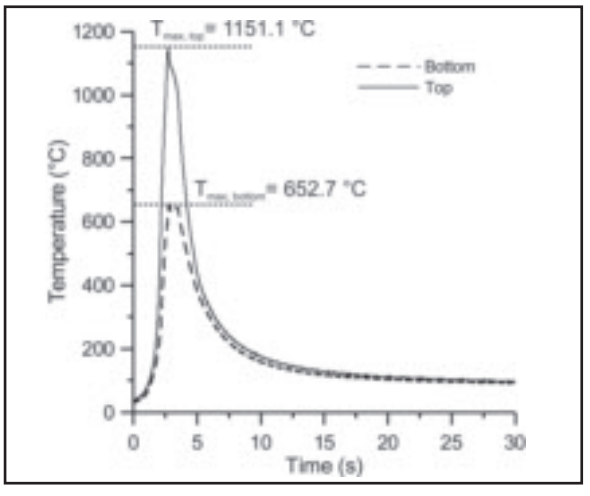

Fig. 5 — Typical temperature vs. time profiles measured during laser brazing at the top and bottom side of the joint.

equipped with an EDS.

As shown in Fig. 2B, 5-mm-wide rectangular-shaped specimens were cut from the brazed joints and subjected to tensile-shear tests with a crosshead speed of 1 mm/min. Shims were used at each end of the specimens to ensure shear loads in the lap joint while minimizing induced couples or bending of the specimens. Average tensile shear strength was calculated from tensile specimens to estimate the static mechanical resistance and joint efficiencies of the joints.

Results

A photograph of a laser-brazed Ni electroplated steel/AZ31B joint and a typical cross-sectional view of the joint are shown in Fig. 3. This brazed joint was made using 2.2 kW laser power, 8 mm/s travel speed, and 0.2 mm beam offset to the steel side. The joint exhibited a uniform brazed area with good wetting of both base materials. Partial melting of the AZ31B base metal was observed. In contrast, when bare steel was used, no bonding occurred between the steel sheet and the braze alloy fusion zone (FZ) and wetting of the steel by the braze metal was very poor (Ref. 15). The 5.5-μm-thick Ni electrodeposited layer on the surface of the steel significantly improved the wetting of the steel by molten

Mg-Al filler metal. Detailed microstructural analysis of the fusion zone and AZ31B Mg alloy after the laser brazing process has been reported in our previous investigation (Ref. 15). This paper focuses on microstructural analysis of the steel-fusion zone interface.

Microstructural Evolution along the Steel-FZ Interface

Figure 4 shows the microstructure at different locations of the steel-FZ interface. The Ni coating was not detected as a separate layer along the interface after the LBP, which would suggest that it had entirely melted and gone into solution in the liquid immediately adjacent to the interface. It was observed that the microstructure of the FZ-steel interface changed significantly across the FZ-steel interface from the bottom (Position A, Fig. 4B) to top (Position F, Fig. 4E) side of the joint. In order to explain this change of microstructure during the laser brazing process, temperature distribution across the interface vs. time was measured during laser brazing using two thermocouples, one attached to the top side and the other to the bottom side of the steel sheet (see Fig. 2A). According to the measured temperature profiles shown in Fig. 5, the steel sheet experienced maximum temperatures of 1151.1° and 652.7°C on the top and the bottom side, respectively. Therefore, a 500°C temperature gradient was measured between the top and bottom side of the steel sheet during the laser brazing process, since the laser beam was focused on the top of the filler metal, as shown in Fig. 2A (Ref. 15). This temperature difference and gradient across the joint interface during the laser brazing process is believed to be the main reason for the prominent change of microstructure across the FZ-steel interface.

As shown in Fig. 4B, at the bottom of the interface a few diamond-shaped bright phases were formed near the steel-FZ interface. In order to identify these phases, a TEM foil was prepared from position B of Fig. 4A. Figure 6 shows the TEM images, EDS plot, and selected area diffraction pattern (SADP) of these submicron particles. The diffraction pattern shows a standard diffraction pattern of AlNi (with BCC structure) with [011] zone axis of the particle. According to an EDS analysis of the diamond-shaped bright phases shown in Fig. 4B, the composition of the particles was 49.6 ± 1.3 at.-% Ni, 45.4 ± 4.7 at.-% Al, and 5.0 ± 2.5 at.-% Mg, thus confirming that the diamond-shaped particles were mainly composed of AlNi intermetallic compound (IMC). Representative concentration profiles of Ni, Al, and Mg across one AlNi particle are shown in Fig. 6D, which indicates that a trace amount of magnesium was found in this particle. It has been reported that each of the Al-Ni binary intermetallics has some solubility for substitutional magnesium atoms (Ref. 19).

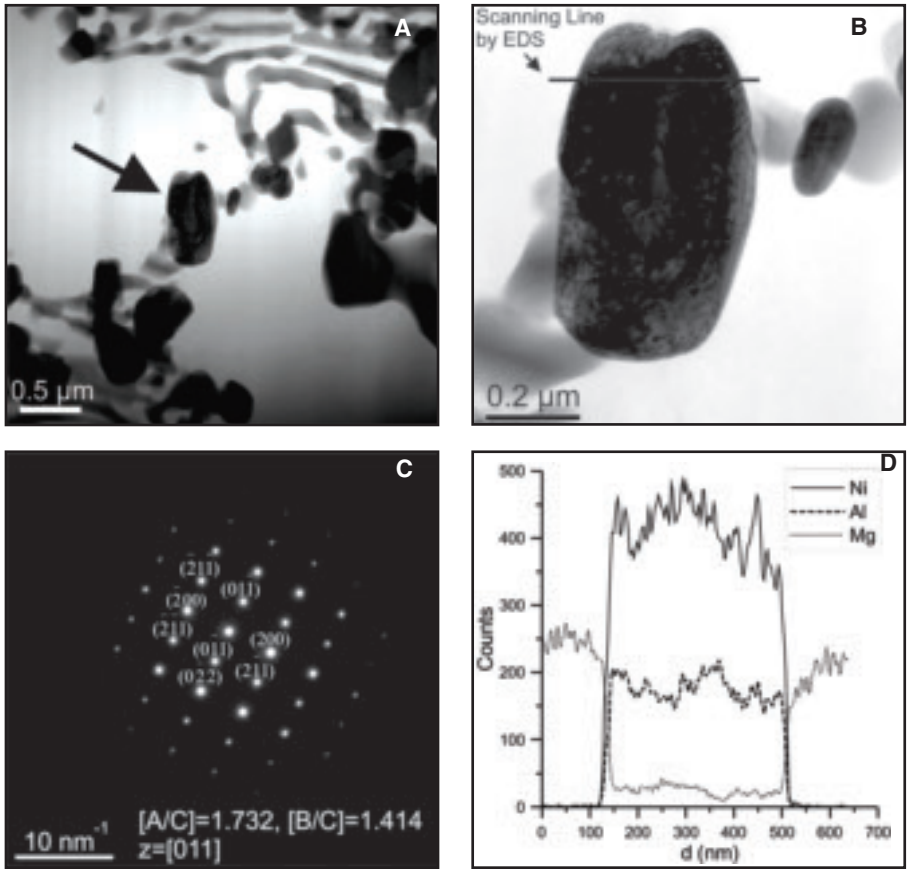

Fig. 6 — AlNi particle characterization at position B shown in Fig. 4A: A, B — TEM images; C — SADP in the [011] zone axis of this particle; D — EDS composition line scans across an AlNi particle indicating line scans of Ni, Al, and Mg.

Figure 7 shows the XRD spectra obtained from the middle of the steel-FZ interface. The area covered by the X-ray beam was a 300-μm-diameter circle. This XRD result confirmed the existence of AlNi IMC, Fe, β-$Mg_{17}Al_{12}$, and α-Mg. The AlNi IMC compound was not found at the middle of the FZ area, whereas the XRD pattern in Fig. 7 showed some weak peaks suggesting that AlNi IMC had formed mainly at the steel-FZ interface.

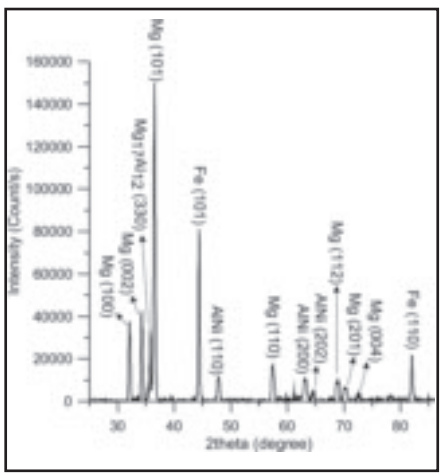

Fig. 7 — X-ray diffraction pattern of the steel-FZ interface.

It was observed that upon moving from the bottom to the middle of the interface, which was associated with increasing temperature, the morphology of the IMC phase along the interface changed from the diamond-shaped AlNi to a faceted dendritic-shaped phase (see Fig. 4C, D).

Energy-dispersive X-ray spectrometer analysis results indicated this dendritic phase contained 43.0 ± 1.6 at.-% Ni, 52.1 ± 2.0 at.-% Al, and 4.9 ± 0.5 at.-% Mg. This composition again corresponded with the AlNi IMC phase. In this area, the first precipitated phase from the liquid was AlNi IMC, the same as at the bottom of the joint. This phase grew steadily in a faceted dendritic shape. As the interface temperature increased with moving from position A to position E in Fig. 4A, the growth morphology of the AlNi phase changed from diamond-shaped to a faceted dendritic shape, as demonstrated in Fig. 4D. Continuous growth of the AlNi was observed in this area with some dendrites having long secondary dendrite arms (see Fig. 4D).

At the top of the joint (position F in

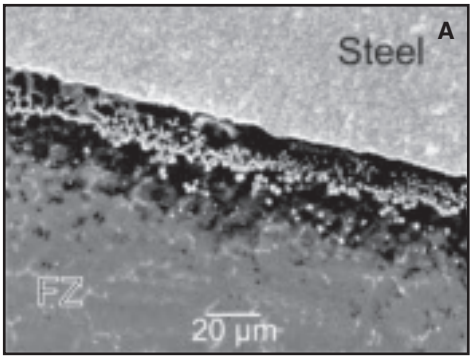

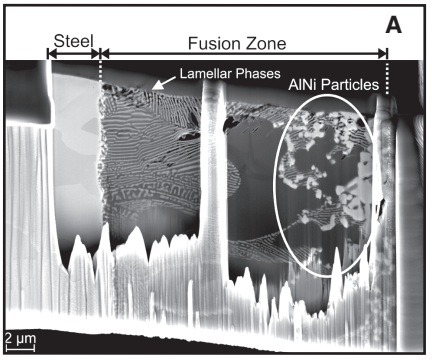

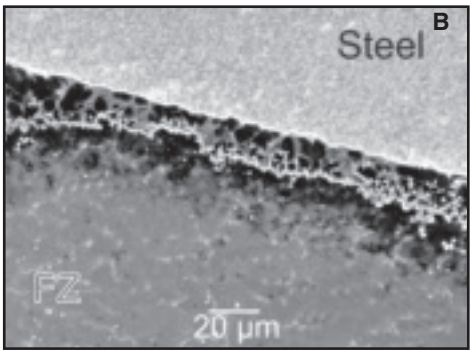

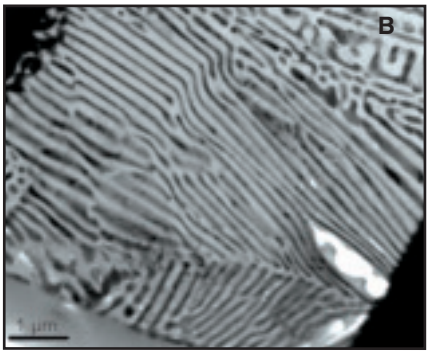

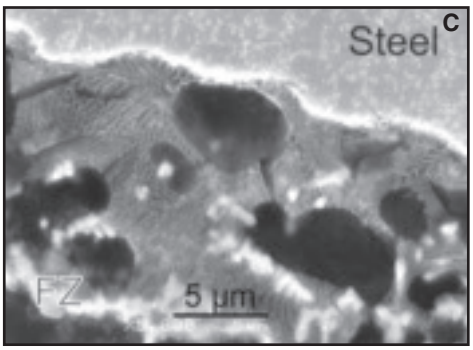

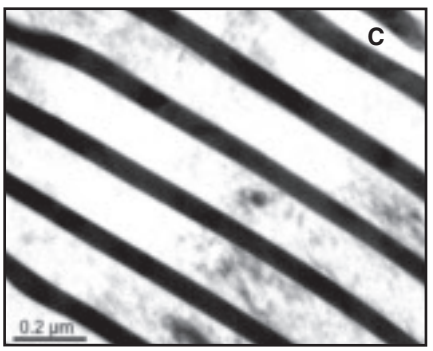

Fig. 8 — SEM images of the steel-FZ interface show the solidification morphology of remaining melt between the IMC layer and steel side: A — Position A in Fig. 4A near bottom side; B — position B in Fig. 4A; C — Mg-Mg_2Ni eutectic phases.

Fig. 9 — A — TEM sample attached to a copper grid; B, C — TEM images of the lamellar phases formed along the steel-FZ interface.

Fig. 4A), the morphology of the interfacial phase changed further and a high volume fraction of a particle-like phase with the composition of 48.4 ± 1.4 at.-% Ni, 50.1 ± 1.2 at.-% Al, and 1.5 ± 0.4 at.-% Mg was detected (Fig. 4E). This phase was also found to be AlNi IMC phase. It should also be noted that formation of the AlNi phase consumed almost all of the Al content of the melt near the steel-FZ interface. Thus, no β-$Mg_{17}Al_{12}$ was observed near the interface compared with the central part of the FZ.

Solidification of the Remaining Melt between the AlNi IMC Phase and Steel

At the bottom of the joint, AlNi IMC first crystallized from the liquid close to the interface and then supersaturated α-Mg solid solution containing 10.6 ± 3.6 at.-% Ni, 3.2 ± 1.7 at.-% Al, and 2.9 ± 1.5 at.-% Fe (dark regions in Figs. 4B and 8) solidified from the liquid during cooling along with the AlNi phase. In some locations between the bottom and middle of the interface, some gray lamellar phases, as shown in Figs. 8C and 9, were also observed between the AlNi IMC layer and the steel. Figure 9A shows the position of AlNi precipitates with respect to the steel-fusion zone interface in the prepared sample during focused ion beaming for TEM analysis. Figure 9B, C shows TEM images of this lamellar (plate-like) phase. According to EDS analysis, the white lamellae corresponded to α-Mg and the dark lamellae containing 27.6 ± 7.2 at.-% Ni and 72.3 ± 7.3 at.-% Mg represented the Mg_2Ni stoichiometric intermetallic compound (also confirmed by SADP analysis). Based on these results, these two phases next to each other are the Mg-Mg_2Ni lamellar eutectic.

Formation of the Mg-Mg_2Ni lamellar eutectic was not uniform and continuous along the interface. As shown in Fig. 8A, B, in some locations between the steel and the AlNi IMC layer, Mg_2Ni crystallized in the form of a lamellar gray phase and in other locations it was not seen and a dark solid solution of Mg containing small amounts of Ni, Al, and Fe was formed. In the middle portion of the interface, the AlNi phase crystallized first in the liquid (Fig. 4D). Then, dark α-Mg solid solution containing 5.8 ± 2.1 at.-% Ni, 1.2 ± 0.3 at.-% Al, and 3.1 ± 0.5 at.-% Fe formed during cooling along with AlNi phase. Finally, at the top of the joint, the AlNi phase precipitated heavily in the liquid along the interface and then the remaining liquid solidified during cooling in the form of α-Mg solid solution (containing 2.4 ± 0.6 at.-% Ni, 0.3 ± 0.1 at.-% Al, and 3.4 ± 0.3 at.-% Fe) along with and among AlNi particles (see Fig. 4E). Upon moving from the bottom to the top of the interface, the Fe content of the remaining liquid between AlNi IMC and the steel increased from 2.9 to 3.4 at.-% due to more diffusion of Fe from the steel side to the FZ at higher temperature. In contrast, Al and Ni showed opposite behaviors due to an increase in the thickness of AlNi IMC from the bottom to the top portion of the joint (from 5 to 30 μm).

Transition Layer

Based on the TEM analysis, the AlNi phase did not grow epitaxially on the steel substrate, but instead nucleated and grew in the liquid adjacent to the interface and was surrounded by either α-Mg + Mg_2Ni eutectic phases or just α-Mg phase close to the interface. On the other hand, while it may appear in Fig. 8 that all of the electroplated Ni had melted and gone into solution in the liquid and the α-Mg may have nucleated and grown epitaxially from the steel surface, it is well known that Mg and Fe are an immiscible couple. From a crystallographic point of view, it is not possible for magnesium to nucleate on steel due to the very large lattice mismatching of Fe and Mg (Ref. 4). Therefore, another layer or phase must be responsible for bonding between the steel and fusion zone.

Further high-magnification microstructural analysis of the steel-fusion zone interface was performed by TEM to find an explanation for the observed interfacial phases. Figure 10A shows a TEM image of the steel-fusion zone interface. A continuous nano-interlayer (50–200 nm thick) phase was observed along the interface, which was bonded to the steel side on one side and to the fusion zone on the other side. Higher magnification of this

layer (as shown in Fig. 10B) confirmed good coherency between this layer and steel as well as the fusion zone. According to EDS point analysis, the Ni content of the transition layer varied between 17 and 40 at.-%. Figure 10C shows the selected area diffraction pattern (SADP) on the transition layer that identified it as Fe(Ni) solid solution with face-centered cubic (FCC) structure. Therefore, this layer proved to be the key factor for realizing a metallurgical bond between the steel and fusion zone. Representative concentration profiles of Fe, Ni, and Mg across the interface between the fusion zone and the steel are shown in Fig. 10D. It is evident from these line scans that Fe, Ni, and Mg diffused into each other as a result of the high temperature experienced during the laser brazing process. As a result, two diffusion or transition layers formed between the steel and fusion zone. According to the element distributions of Fe, Ni, and Mg (see Fig. 10D), in transition layer I with a thickness of almost 70 nm from the steel side, the Fe content decreased gradually while the Ni content increased. In this layer, solid-state diffusion of Ni and Fe into each other is believed to control the overall thickness of this layer.

Another diffusion layer (transition layer II) was observed in Fig. 10D between the transition layer I and the fusion zone. The thickness of this layer was ≈ 60 nm. A slight diffusion of magnesium from fusion zone into transition layer II was detected. It would appear that there was sufficient solubility of the Mg in this Fe(Ni) interlayer for diffusion of the Mg to occur and that wetting and bonding of the α-Mg + Mg_2Ni eutectic phases had in fact occurred with the thin Fe(Ni) interlayer that had formed during laser brazing, and not directly with the steel.

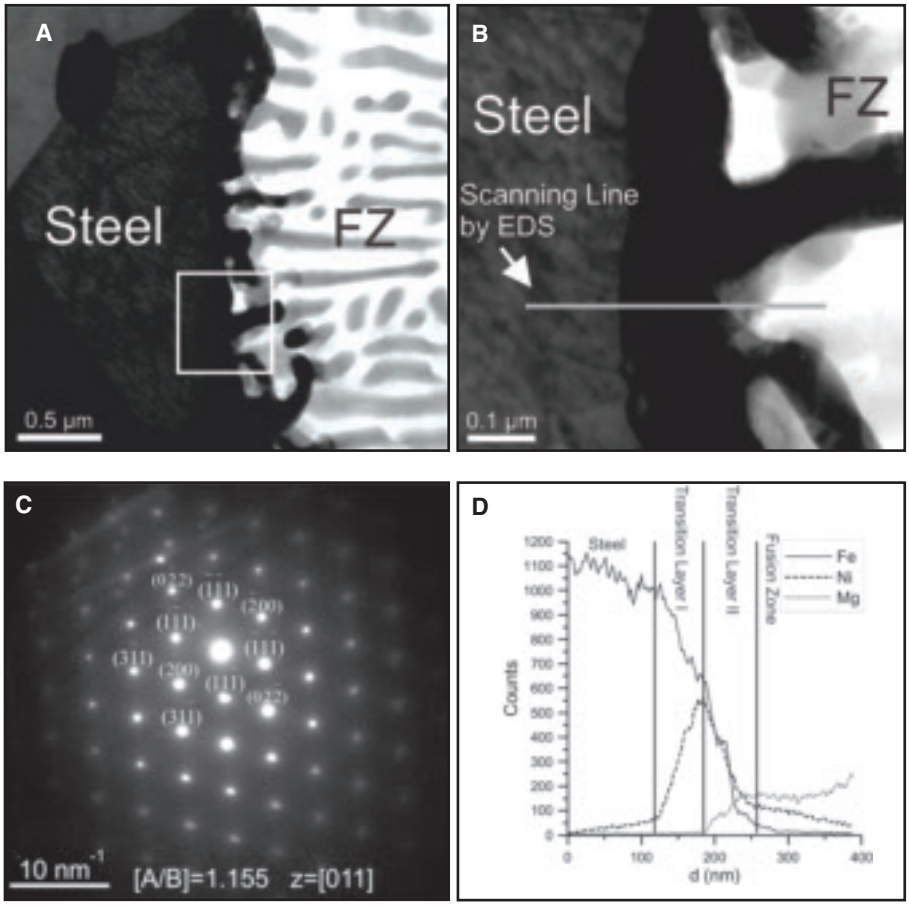

Fig. 10 — A— TEM image of the steel-fusion zone interface; B— higher magnification of the selected square area in A; C — SADP in the [011] zone axis of the interfacial phase; D — EDS line scan analysis of Fe, Ni, and Mg at the steel-fusion zone interface.

Mechanical Properties

Due to the nonsymmetric configuration of the 5-mm-wide tensile-shear test specimens (see Fig. 2B), a combination of shear and tensile forces existed at the interface. Consequently, the joint strengths are reported here as fracture load, since it is not possible to separate tensile and shear stresses. The average tensile shear strength of the laser brazed steel-Ni-AZ31B joints using the Mg-Al filler metal was found to be 153.7 ± 2.7 kgf (or 1506.3 ± 24.5 N). This is 153% higher than tensile shear strength of the laser brazed Al-coated steel-AZ31B Mg alloy specimens obtained in our previous study (Ref. 15). The low standard deviation of the tensile shear strength of the laser brazed steel-Ni-AZ31B joints (±2.7 kgf) compared with the laser brazed steel-Al-AZ31B joints (±11 kgf) indicated that the laser brazing process was inherently stable and reproducible. If only the shear plane is considered, the average shear strength of the joints was 96.8 MPa, or 60% of that of AZ31B-H24 Mg alloy base metal.

All tensile-shear specimens fractured in the FZ very close to the steel-FZ interface. Typical fracture surfaces of both the fusion zone side and steel side after tensile shear testing are shown in Fig. 11. Figure 11A, C are low-magnification SEM micrographs of the fracture surfaces of the fusion zone side and steel side, respectively, and dimples are shown at high magnification in Fig. 11B, D. This uniform distribution of the dimples is characteristic of ductile fracture surfaces. These fracture surfaces indicated that the specimens failed under conditions similar to tensile test with a strong shear stress component (tensile-shear test). The effect of shear stress on the morphology of the dimples is very evident in these micrographs. The vertical direction in each of the micrographs is parallel to the direction of the shear, and the elongation of the dimples under the action of shear stress is evident in Fig. 11B, D. The AlNi IMC compound was not found at the fracture surfaces.

The EDS analysis results of the fracture surfaces of both the steel and FZ side also indicated that crack propagation during the tensile shear tests had occurred entirely in the FZ. Based on the EDS results, the composition of the fracture surface for both steel side and FZ side were similar to the FZ, meaning fracture passed through the FZ near the steel-FZ interface.

Figure 12 shows the XRD pattern from the fractured surface of the joint on the steel side. Fe, α-Mg, and AlNi peaks were seen in this X-ray diffraction result. These findings were consistent with the SEM and EDS analysis results.

Discussion

From the above results, the interaction between the filler metal and surface of the Ni-plated steel can be explained as follows (see Fig. 13):

Firstly, the solid-state Ni-plated steel is in contact with the liquid filler metal (Mg-Al alloy) at the laser brazing temperature and, subsequently, the liquid Mg-Al alloy flows over the Ni surface — Fig. 13A.

Secondly, dissolution and diffusion of Ni atoms into the liquid occur, as shown in Fig. 13B. At the same time, some solid-state diffusion of Ni atoms into the steel also occurs. A slight diffusion of Fe atoms

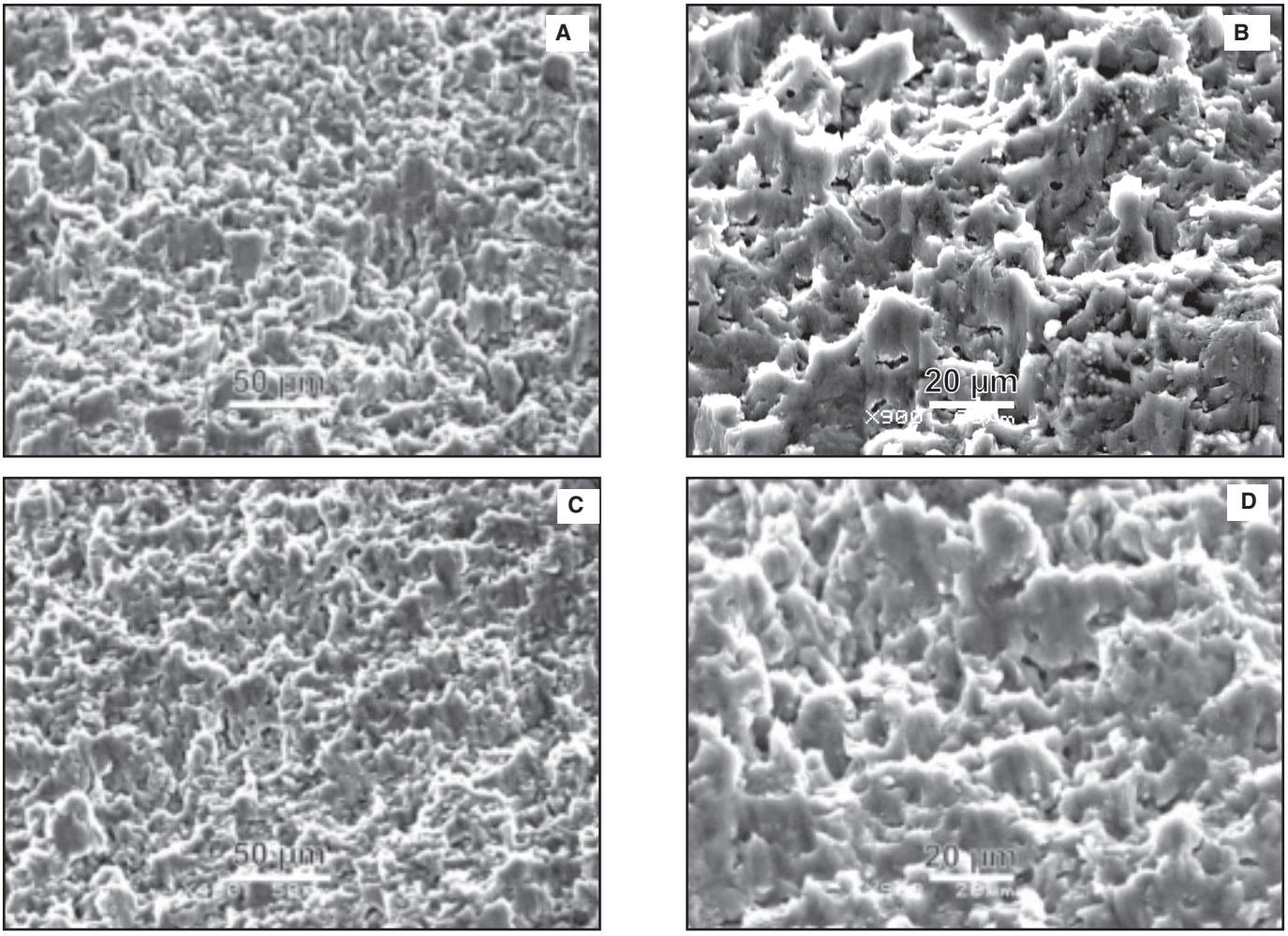

Fig. 11 — SEM images of typical fracture surfaces after the tensile shear test. A, B — Fusion zone side at different magnifications; C, D — steel side at different magnifications.

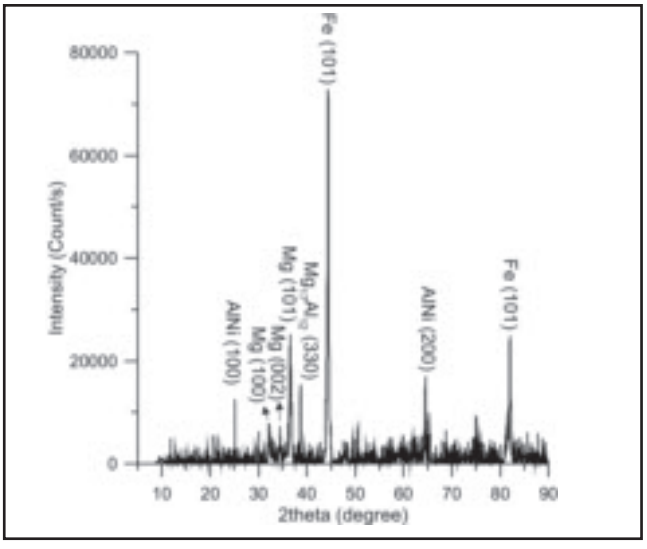

Fig. 12 — X-ray diffraction pattern of the fracture surface of the steel side.

into the liquid was also observed. Meanwhile, Mg atoms from the liquid may slightly diffuse into the Ni-alloyed steel side. Therefore, a thin diffusion or transition layer forms continuously along the interface between steel and fusion zone from the bottom side to the top side of the joint. This transition layer is a solid solution of Ni in Fe (with low content of Mg for transition layer II). This Fe(Ni) solid solution with FCC crystal structure is more favorable for bonding to Mg than having a body-centered cubic (BCC) phase along the interface. Zhang et al. (Ref. 20) used an edge-to-edge matching crystallographic model to predict all orientation relationships between crystals that have simple hexagonal close-packed (HCP) and BCC structures, and they found that the lattice mismatching of HCP (Mg) and BCC (Fe) is very large. On the basis of the observation in our study, a diffusion layer composed of Fe and Ni with FCC structure can provide the conditions for the heterogeneous nucleation of α-Mg during solidification. The result is formation of a metallurgical bond between the steel and magnesium alloy. A recent study by Liu et al. (Ref. 4) showed that a nano-layer of Fe_2Al_5 on steel can also be a transition layer to bond Fe to Mg due to the low energy interfaces and good match of lattice sites between Fe and Fe_2Al_5 as well as Mg and Fe_2Al_5. The same behavior was observed for the Fe(Ni) transition layer in this study. Formation of a transition zone was also reported in other studies (Refs. 5–8) using different joining techniques, when an interlayer was used between steel and Mg alloy. These transition layers on steels were reported to make it possible to join Mg and steel.

Thirdly, during the solidification process, the AlNi phase with a high melting point (1133°C) precipitates from the liquid and grows in a form of faceted dendrites very close to the interface — Fig.

13C. These faceted dendrites form due to kinetic difficulties in forming new planes of atoms (Ref. 21). In this type of dendrite, the growing direction of dendrite arms are ones that are capped by relatively slow growing planes (usually low-index planes) (Ref. 21). The slowest growing plane would be expected to be the closest-packed planes. Weinberg and Chalmers (Ref. 22) reported that the axis of a pyramid, whose sides are the most closely packed planes, is generally the major dendrite direction. As a result, for AlNi faceted dendrites with BCC structure, this direction is <100>. Therefore, the process of solidification at the middle part of the joint starts with the nucleation and growth of the AlNi-faceted dendrites along the <100> growth direction.

Fourthly, if the Ni content of the remaining liquid between the steel side and formed AlNi precipitates is high enough, Mg_2Ni with a melting point of 762°C nucleates (see Fig. 13C). Formation of Mg_2Ni depends on sufficient Ni concentration in the remaining liquid near the steel-FZ interface after formation of the AlNi IMC. The Ni content of the remaining liquid after precipitation of AlNi increases from 2.4 at.-% at the top side of the interface to 10.6 at.-% at the bottom portion because formation of the AlNi IMC layer consumed the Ni atoms near the interface and the volume fraction of this phase increased from the bottom to the top portion of the joint.

Based on the above analysis, high enough concentration of Ni in the remaining liquid close to the bottom side of the joint after formation of AlNi IMC resulted in formation of the Mg_2Ni + α-Mg lamellar eutectic in the form of a gray phase between the AlNi IMC and steel. In order for this lamellar eutectic to grow, the local composition of the fusion zone should be close to the eutectic composition (10 at.-% Ni, according to the Mg-Ni binary phase diagram) (Ref. 21). Reactions between Mg in the fusion zone and Ni along the interface caused formation of the Mg-Ni eutectic phase. This reaction can be represented by the following balanced chemical reaction:

$$L(10\ at.\text{-}\%\ Ni) \leftarrow 508°C \rightarrow Mg_2Ni\ (33\ at.\text{-}\%\ Ni) + Mg(0\ at.\text{-}\%\ Ni) \qquad (1)$$

Therefore, at the bottom of the interface, two reactions occurred; the first one was precipitation of AlNi from the liquid and the second was the eutectic reaction between Mg and Ni in the FZ (reaction 1). In the case of reaction sequences, first AlNi forms near the interface and then the remaining liquid with a low Al content between the AlNi IMC and steel-FZ interface, which is still rich in Ni, undergoes a eutectic reaction with Mg and results in the formation of the lamellar α-Mg + Mg_2Ni eutectic.

With the formation of the AlNi IMC layer, diffusion of Ni atoms from the steel side to the FZ is blocked. Therefore, the concentration of Ni in the remaining liquid between the interface and preformed AlNi phase is expected to be higher than the remaining liquid on the other side of the AlNi phase. The result is the formation of Mg_2Ni just between the AlNi phase and steel (see Fig. 8A, B).

In the top portion of the interface, with the nucleation and growth of the AlNi particles, most of the Ni atoms are consumed. Therefore, the Ni content of the remaining liquid would not be enough for formation of the Mg_2Ni phase.

Conclusions

1. With the addition of an electrodeposited Ni interlayer on steel sheet, single flare bevel lap joints of AZ31B-H24 Mg alloy to steel sheet were rendered possible by the laser brazing process, and a uniform brazed area with good wetting and bonding of both base metals was achieved.

2. Dissolution of the Ni coating layer during the laser brazing process led to the formation of new AlNi IMC phases and also a Mg-Ni eutectic zone along the interface. The AlNi intermetallic layers at the steel-FZ interface formed in the sequence of diamond-shaped, dendritic, and nodules from the bottom to the top portion of the joint.

3. The formation of a nano-scale Fe(Ni) transition layer on the steel by solid-state interdiffusion between Fe and Ni during laser brazing was found to be responsible for the formation of a metallurgical bond between the steel and the Mg-Al brazing alloy.

4. The average shear strength of the joints reached 96.8 MPa, 60% that of the base metal of AZ31B Mg alloy. Fracture surface analysis showed that fracture occurred in the FZ close to the steel-FZ interface.

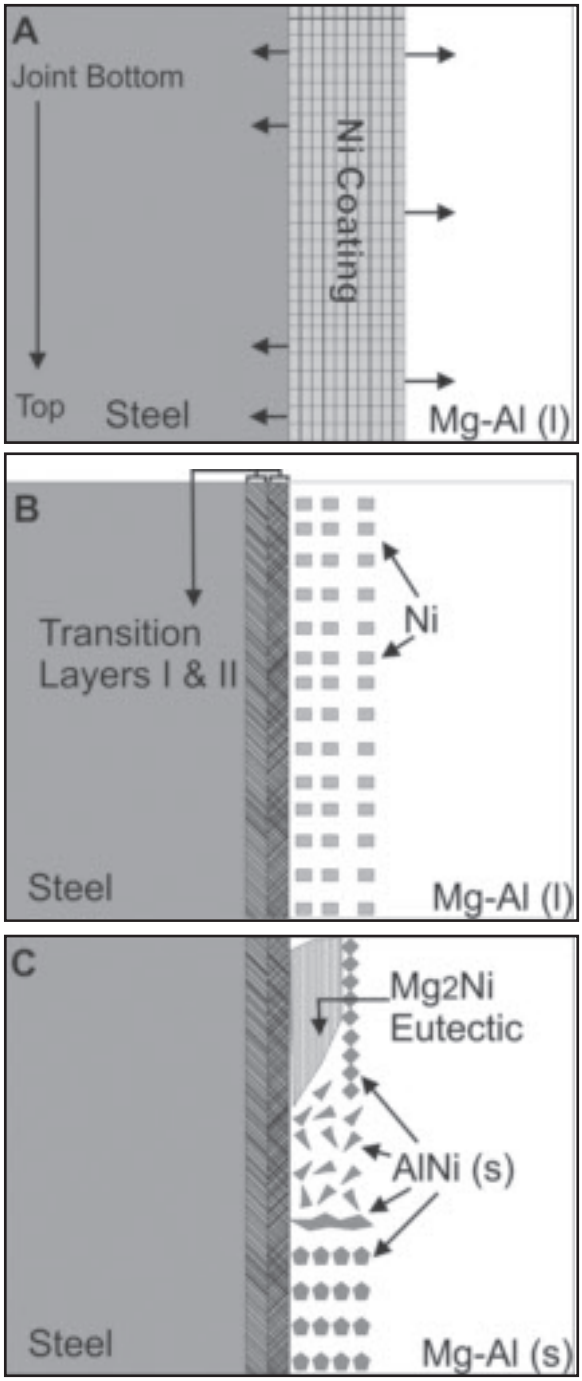

Fig. 13 — Formation of transitional layer and intermetallic compounds during laser brazing of Ni-plated steel-AZ31B with Mg-Al filler metal: A — Wetting of the Ni-plated steel by molten filler metal and dissolution and diffusion of Ni into the FZ and steel substrate; B — formation of the transitional layer and aggregation of Ni along the interface; C — nucleation and growth of AlNi IMC, and epitaxial growth of the remaining liquid in the form of α-Mg + Mg_2Ni eutectic onto the thin Fe(Ni) interlayer.

Acknowledgments

The authors wish to acknowledge support of the American Welding Society (AWS) Graduate Fellowship program, the Natural Sciences and Engineering Research Council of Canada (NSERC), and

Magnesium Network of Canada (MagNET) for sponsoring this work. The authors would like to acknowledge the helpful comments of Dr. Scott Lawson from the Centre for Advanced Materials Joining at the University of Waterloo.

References

1. Yan, J., Xu, Z., Li, Z., Li, L., and Yang, S. 2005. Microstructure characteristics and performance of dissimilar welds between magnesium alloy and aluminum formed by friction stirring. *Scripta Materialia* 53: 585–589.

2. Mao, H. K., and Bell, P. M. 1979. Equations of state of MgO and Fe under static pressure conditions. *Journal of Geophysical Research* 4533–4536.

3. Liu, L. 2005. *Welding and Joining of Magnesium Alloys*, Cambridge, UK: Woodhead Publishing Ltd.

4. Liu, L., Xiao, L., Feng, J., Li, L., Esmaeili, S., and Zhou, Y. 2011. Bonding of immiscible Mg and Fe by coated nanoscale Fe_2Al_5 transition layer. *Scripta Materialia* 65 (11): 982–985.

5. Zhao, X., Song, G., and Liu, L. 2006. Microstructure of dissimilar metal joint with magnesium alloy AZ31B and steel 304 for laser-tungsten inert gas lap welding. *Transactions of China Welding Institution* 27: 1253–1256.

6. Qi, X., and Song, G. 2010. Interfacial structure of the joints between magnesium alloy and mild steel with nickel as interlayer by hybrid laser-TIG welding. *Materials & Design* 31: 605–609.

7. Liu, L., Xiao, L., Feng, J. C., Tian, Y. H., Zhou, S. Q., and Zhou, Y. 2010. The mechanism of resistance spot welding of magnesium to steel. *Metallurgical and Materials Transactions A* 41A: 2651–2661.

8. Liu, L., Qi, X., and Wu, Z. 2010. Microstructural characteristics of lap joint between magnesium alloy and mild steel with and without the addition of Sn element. *Materials Letter* 64: 89–92.

9. Liu, L. M., and Qi, X. 2009. Effects of copper addition on microstructure and strength of the hybrid laser-TIG welded joints between magnesium alloy and mild steel. *Journal of Materials Science* 44: 5725–5731.

10. Lockwood, L., and Shapiro, A. E. 2005. Brazing of magnesium. *Brazing Handbook*, 5th edition, Miami, Fla.: American Welding Society.

11. Sierra, G., Peyre, P., Deschaux Beaume, F., Stuart, D., and Fras, G. 2008. Steel to aluminium braze welding by laser process with Al-12Si filler wire. *Science and Technology of Welding and Joining* 13(5): 430–437.

12. Wagner, F., Zerner, I., Kreimeyer, M., Seefeld, T., and Sepold, G. 2001. Characterization and properties of dissimilar metal combinations of Fe/Al and Ti/Al-sheet materials. *Proc. ICALEO'01 (CD-ROM)*, Jacksonville, Fla., October, LIA, Orlando, Fla.

13. Miao, Y., Han, D., Yao, J., and Li, F. 2010. Microstructure and interface characteristics of laser penetration brazed magnesium alloy and steel. *Science and Technology of Welding and Joining* 15(2): 97–103.

14. Kreimeyer, M., Wagner, F., and Vollertsen, F. 2005. Laser processing of aluminum-titanium-tailored blanks. *Optics and Lasers in Engineering* 43: 1021–1035.

15. Nasiri, A. M., Li, L., Kim, S. H., Zhou, Y., Weckman, D. C., and Nguyen, T. C. 2011. Microstructure and properties of laser brazed magnesium to coated steel. *Welding Journal* 90(11): 211-s to 219-s.

16. Material Safety Data Sheet. 2003. Superior Flux & Mfg. Co. November 11. p. 1.

17. Saida, K., Song, W., and Nishimoto, K. 2005. Diode laser brazing of aluminum alloy to steels with aluminum filler metal. *Science and Technology of Welding and Joining* 10(2): 227–235.

18. Vander Voort, G. F. 1999. *Metallography Principles and Practice*. Materials Park, Ohio: ASM International.

19. Belov, N. A., Eskin, D. G., and Avxentieva, N. N. 2005. Constituent phase diagrams of the Al-Cu-Fe-Mg-Ni-Si system and their application to the analysis of aluminum piston alloys. *Acta Materialia* 53: 4709–4722.

20. Zhang, M. X., Kelly, P. M., Qian, M., and Taylor, J. A. 2005. Crystallography of grain refinement in Mg-Al based alloys. *Acta Materialia* 53: 3261–3270.

21. Flemings, M. C. 1974. *Solidification Processing*. McGraw-Hill. pp. 157–160.

22. Weinberg, F., and Chalmers, B. 1952. Further observations on dendritic growth in metals. *Canadian Journal of Physics* 30: 488–502.

AWS Expands International Services

With international membership on the rise, the American Welding Society (AWS) launched a series of country-specific Web sites known as microsites for members to access information in their native languages.

Multilingual microsites are now live for Mexico at *www.aws.org/mexico*, China at *www.aws.org/china*, and Canada (English/French) at *www.aws.org/canada*. They feature information on services offered by AWS in each country, membership benefits, exposition information, online education, and access to AWS publications and technical standards.

Other countries will be added later.